Available online at www.sciencedirect.com
ScienceDirect
Ocean Modelling 15 (2006) 90–100
Ocean Modelling
www.elsevier.com/locate/ocemod

Design considerations for a finite element coastal ocean model

Roy A. Walters *

National Institute for Water and Atmospheric Research, P.O. Box 8602, Riccarton, Christchurch, New Zealand

Received 17 March 2005; received in revised form 26 November 2005; accepted 30 November 2005
Available online 3 January 2006

Abstract

Numerical models for flow problems must be adapted to a wide range of physical processes and a corresponding wide range of temporal and spatial scales. The large number of different models is thus not surprising because the models must be tailored to specific problem types. The design considerations presented here are aimed toward coastal ocean models. There are several fundamental choices that must be made: form of the equations, discretisation in time and space, and physics to include. Of these, choice of the specific finite element to use and advection scheme are two longstanding issues. Another pivotal issue is whether to satisfy mass continuity locally, in patches, and/or globally. The choices presented here result in a model that is applicable to a range of coastal problems from short time-scale tsunami propagation and runup, to long time-scale flows.

Keywords: Numerical model; Finite element; Coastal ocean; Tsunami

1. Introduction

Numerical models for flow problems must be adapted to a wide range of physical processes and a corresponding wide range of temporal and spatial scales. The large number of different models is thus not surprising because the models must be tailored to specific problem types. Creation of a general flow solver is probably not feasible due to many constraints, efficiency being an important one.

Coastal ocean models are the focus of the design considerations presented here. Typical length scales are of the order of the continental shelf width and shorter. Typical time scales are of the order of the period of long waves (tens of minutes) and longer. Typical flow features range from tsunami propagation to seasonal baroclinic circulation. Embedded in these flows are short gravity waves which may or may not be of interest.

In forming a model, several fundamental choices must be made at an early stage: choosing the form of the governing equations, choosing a discretisation in time and space, and selecting the particular physical processes to include. Of these, choice of discretisation (element and associated basis functions) and advection

* Tel.: +64 3 348 8987; fax: +64 3 348 5548.
E-mail address: r.walters@niwa.co.nz

1463-5003/$ - see front matter
doi:10.1016/j.ocemod.2005.11.002

scheme are two longstanding issues. Another pivotal issue is whether to satisfy mass continuity locally, in patches, and/or globally. This choice is reflected in the specific element chosen.

In the following sections, these topics are pursued in sequence and specific choices are made. Note that this treatment does not specifically consider the transport equations or the density forcing terms. These equations are solved using finite volume methods that conserve mass locally and this places a constraint on the mass conservation properties of the hydrodynamics part of the model. Solution of the transport equations has received attention from many researches over the years, and the methods used here are similar to those described by Casulli and Zanolli (2005). In Section 6, the model is applied to tsunami propagation and runup along the New Zealand coastal margin as a test of the choices that were made.

2. Form of the governing equations

The governing equations must accommodate a wide range of temporal and spatial scales from global and local forcing down to dissipation scales for turbulence. The Navier–Stokes equation and incompressibility constraint are the standard equations describing the hydrodynamics (Phillips, 1969). However, it is not feasible to solve these equations over the large range of scales so that both time and space averaging (filtering) must be employed. For instance, compare direct numerical simulation (DNS) where no filtering is used, to the Reynolds-averaged Navier–Stokes equation (RANS) where time-averaging is used and to large eddy simulation (LES) where spatial filtering is used (Galperin and Orszag, 1993).

Double averaging over time then space is applied to the Navier–Stokes equation and incompressibility constraint to derive the set of governing equations used here (Finnigan, 2000). The first step, averaging over time, follows the standard procedure used to derive the RANS equation (Phillips, 1969; Monin and Ozmidov, 1985). This leads to the problem of closure where higher-order moments are required to close the equations. A discussion of closures is beyond the scope of this paper; however, considerable research has gone into this area (see Burchard, 2002).

The second step, volume averaging in space, results in a set of equations for the double-averaged variables and again leads to a similar closure problem with spatial moments (Nikora et al., 2001). Consideration of these spatial closures is just beginning.

In the end, the double-averaged Navier–Stokes equations (DANS) account for the unresolved space and time scales in a formal manner, and thus provide a method to include their effects into the model (Nikora et al., 2001). For example, some unresolved effects are from sub-grid scale bottom roughness such as sand waves and other topographic features, sub-grid scale velocity variations, and vegetation when treating long-wave runup.

In tensor form, the equations of momentum and mass conservation are

$$\frac{\partial u_i}{\partial t} + u_j \frac{\partial u_i}{\partial x_j} + 2\varepsilon_{ijk}\Omega_j u_k = -\frac{\partial p}{\partial x_i} - g\delta_{i3} + \frac{\partial \tau_{ij}}{\partial x_j} + F_i \tag{1}$$

$$\frac{\partial u_i}{\partial x_i} = 0 \tag{2}$$

where the convention is used that repeated indices are summed, x_i, $i = 1, 3$ are distances (x, y, z) along the coordinate axes in the east, north, and upward direction, respectively; $u_i(x_i, t)$, $i = 1, 3$ are velocity components (u, v, w) along the coordinate axes; ε_{ijk} is an alternating tensor; Ω_k are the components of the Earth's angular velocity in the local coordinate system; $p(x_i, t)$ is kinematic pressure; g is gravitational acceleration; δ_{ij} is the Kronecker delta which equals 1 if $i = j$ and 0 otherwise; τ_{ij} is stress; and F_i is a body force that includes terms arising from the time and space averaging. Here, the equations are evaluated outside the roughness layer so that the fluid volume and averaging volume are the same (see Nikora et al., 2001) and the equations reduce to a familiar form.

The equation for the free surface η is derived by an integration of the continuity equation over water depth and application of the kinematic free surface and bottom boundary conditions:

$$\frac{\partial \eta}{\partial t} + \frac{\partial}{\partial x}\left[\int_h^\eta u\,\mathrm{d}z\right] + \frac{\partial}{\partial y}\left[\int_h^\eta v\,\mathrm{d}z\right] = \frac{\partial h}{\partial t} \tag{3}$$

where $h(x, y, t)$ is the land elevation measured from the vertical datum, and $H = \eta(x, y, t) - h(x, y, t)$ is the water depth. The vertical datum is arbitrary, but is usually set equal to the average water surface elevation (sea level). This choice minimises truncation errors in the calculation of the water surface gradients. When the bottom is fixed, h is no longer time-dependent and the right-hand side of the equation vanishes.

At this point, there are number of choices to be made in the mathematical model described above. Perhaps the most important of these are the decision whether to use the primitive equations or derived equations, whether to include non-hydrostatic (dynamic) pressure, and determining the closures required for the type of space and time averaging chosen. The description of closures is beyond the scope of this paper.

For the most part, the primitive equations seem to be the most popular choice for the mathematical formulation. On the other hand, derived equations have been used to mitigate the effects of computational modes in certain finite element and finite difference discretisations of the primitive equations. An example of this approach is a finite element model which uses a wave equation formulation (Lynch and Werner, 1991). However, derived equations generally contain higher derivatives which can make discretisation (particularly advection) and boundary conditions more problematic to formulate. Primitive equations are more straightforward to apply, but require a careful choice of methods to avoid spurious modes.

Another major issue is the enforcement of mass conservation. Traditional finite element methods conserve mass locally in a weighted residual sense over the support for a node and also conserve mass globally. This is not a problem as long as the methods are used consistently on all the momentum and transport equations. However, local conservation on an element by element basis is desired here as many of the transport models are formulated with finite volume methods. Use of the primitive equations presents a more direct approach to achieve this.

Following methods described in Casulli (1999), non-hydrostatic pressure can be considered an extension of the methods used for the shallow water equations. First pressure p in (1) is separated into a hydrostatic pressure p_{h} and a dynamic (reduced or non-hydrostatic) pressure $\hat{q}$ such that $p = p_{\mathrm{h}} + \hat{q}$ and by definition

$$\frac{\partial p_{\mathrm{h}}}{\partial z} = -g \quad \text{or} \quad p_{\mathrm{h}} = p_{\mathrm{a}} + g(\eta - z) \tag{4}$$

where p_{a} is kinematic pressure (atmospheric) at the free surface. For hydrostatic flows, $\hat{q} = 0$ and the equations reduce to the shallow water equations. For non-hydrostatic flows there are additional equations to solve for dynamic pressure (Casulli and Zanolli, 2002; Stelling and Zijlema, 2003; Bradford and Sanders, 2002; Lin and Li, 2002). Following this procedure, the appropriate choice can be made based on the problem under consideration.

As a result, the primitive equations given in (1)–(3) will be used as the basis for the mathematical model and the non-hydrostatic extension is described by (4) and in the references.

3. Time discretisation

Both explicit and implicit methods can be used in the solution of Eqs. (1)–(3). By definition, semi-implicit will mean that some of the terms in the equations are treated implicitly and some explicitly. Implicit will mean that a term is approximated in the time interval $[n, n+1]$ by the weight θ where $F^{n+\theta} = \theta F^{n+1} + (1-\theta)F^{n}$ such that $\theta = 0$ is an explicit approximation and $\theta = 1$ is a fully implicit approximation.

The objective is to choose these methods in such a way as to enhance model accuracy, remove restrictive stability constraints, and enhance model efficiency by removing computational overhead. All of these cannot be optimised simultaneously; nonetheless, certain choices are very advantageous (Casulli, 1990; Casulli and Cattani, 1994).

For explicit methods, the two most restrictive stability constraints are the CFL condition for gravity waves and the viscosity constraint on the vertical viscous terms. Hence, the divergence term in (3) and the gravity and vertical viscosity terms in (1) are treated implicitly thereby removing the stability constraints (Casulli and Cattani, 1994). Note, however, that there are still accuracy constraints that limit the magnitude of the CFL number ($\mathrm{CFL} = c\Delta t/L$). The Coriolis term is treated implicitly with a two-step method (Casulli and Walters, 2000) so that this term appears in the equations as an explicit term with a modified coefficient and hence does not impact the matrix solution. The horizontal stresses have weak stability constraints so they are treated explicitly. Treating horizontal stresses implicitly would require the solution of a full three-dimensional matrix for velocity with considerable computational overhead. As will be seen in the following section, the problem is reduced to the calculation of tri-diagonal matrices at each node with a commensurate computational saving.

At this stage, the equations become

$$\frac{\partial \eta}{\partial t}+\frac{\partial}{\partial x}\left[\int_h^\eta u\,\mathrm{d}z\right]^{n+\theta}+\frac{\partial}{\partial y}\left[\int_h^\eta v\,\mathrm{d}z\right]^{n+\theta}=0 \tag{5}$$

$$\frac{\mathrm{d}u_i}{\mathrm{d}t}+2\varepsilon_{ijk}\Omega_j u_k^{n+\theta}=-\frac{\partial p^{n+\theta}}{\partial x_i}-g\delta_{i3}+\left[\frac{\partial \tau_{ij}^n}{\partial x_j}\right]_{j=1,2}+\frac{\partial \tau_{i3}^{n+\theta}}{\partial x_3}+F_i^{n+\theta} \tag{6}$$

Treatment of the advection terms is always a significant problem because of the wide range of flow conditions that may be encountered. Again, explicit methods are chosen in order to avoid solving a large matrix for velocity. Leonard (2002) discusses the construction of unconditionally stable explicit advection schemes and this subject will be dealt with in the following section when discretisation methods are treated.

Finally, it is advantageous to solve the dependent variables sequentially rather than simultaneously in order to make the model more efficient. This is an old idea in fluid dynamics and has been used to generate analytical solutions, is used in the creation of harmonic shallow water models (Walters, 1992; Le Provost et al., 1978), in the wave equation formulation (Lynch and Gray, 1979), and some time-stepping models (Casulli, 1990). To implement this procedure here, the momentum equation (6) is inverted to derive u_i^{n+1} and this expression is substituted into the free surface equation (5) to derive an equation that only involves η at the $n+1$ time level (Walters and Casulli, 1998; Casulli and Walters, 2000). An important note is that a wave equation is formed from the discrete equations with the consequence that any spurious modes contained in the discretisation of the primitive equation are retained. Hence, it is crucial to choose finite elements and bases that do not support spurious modes. This is the subject of the following section.

4. Space discretisation

At some point in the past, the choice of discretisation method (finite difference, finite element, or finite volume) determined the type of computational grid (structured squares or unstructured triangles and quadrilaterals). However, the choice is much wider now as all methods have been used successfully with both types of grid. Hence, the real consideration is obtaining proper resolution of the important topographic variability in a problem. Here, unstructured grids are chosen because of their ability to resolve the complicated and multi-scale geometry of coastal environments.

The basic computational cell is a tessellation using arbitrary quadrilaterals or triangles in the horizontal, and the projection of the nodes (corners) in the vertical to derive brick or pie shaped elements. In general, the vertical grid lines must be parallel to the gravity vector in order to avoid spurious circulations caused by truncation errors as shown by King et al. (1974). For this reason, other 3D elements such as tetrahedra may introduce serious errors.

There are few elements (with associated interpolation functions) that can satisfy the constraints of mass conservation on an element by element basis and yet contain no spurious computational modes. This has been an area of vigorous research for some time (Sani et al., 1981; Walters and Carey, 1984; Hua and Thomasset, 1984; Le Roux et al., 1998; Hanert et al., 2002).

For pure hydrodynamic problems where the requirement for local mass conservation can be relaxed, there are many more options for elements and methods (Walters, 2005a). One alternative is to use the primitive equations in conjunction with the $P_1^{\mathrm{nc}}-P_1$ element (Hua and Thomasset, 1984; Hanert et al., 2005). The advantage of this element is greater accuracy than P_0 elements, and the disadvantage is increased bandwidth in the matrix solver for semi-implicit methods (in addition to the lack of local mass conservation).

In the end, the Raviart–Thomas element of lowest order (Raviart and Thomas, 1977) was found to be the most useful for a coastal ocean model. The horizontal approximation for this element uses piecewise constant bases for pressure and piecewise linear bases for the normal component of velocity which is constant on each edge (Walters and Casulli, 1998). Vertical velocity is piecewise constant on the top and bottom face of an element. This element is the finite element equivalent of the C-grid used in finite difference methods and has similar properties. The element has no spurious gravity wave modes and the use of a normal velocity eases specification of land boundary conditions, wetting and drying conditions, and wave radiation conditions. The element can contain spurious f-modes in velocity depending on the treatment of the Coriolis term, a property similar to the C-grid (Walters and Carey, 1984). However, there is usually no significant development of these modes so they are not an issue (Hanert et al., 2002).

For this element the free surface equation (5) is expressed in weighted-residual form. Because the basis function for η is piecewise constant, the equation reduces to a finite volume form that conserves mass both locally and globally

$$A_e \frac{\partial \eta_e}{\partial t} + \oint_{\Gamma_e} (\mathrm{Hu}_n)\, \mathrm{d}\Gamma_e = 0 \tag{7}$$

where subscript e denotes the value for a specific element; A_e is the element area; u_n is the normal velocity on an edge, positive outwards; and Γ_e is the boundary of the element. The last term has been converted from a divergence form to a line integral using the Gauss Divergence Theorem.

It is worth noting that this finite volume form for the free surface and continuity equation is used in many finite element, finite difference, and of course all finite volume models. The major difference between these types of models is the method by which gradients and fluxes are calculated. For instance, compare the unstructured grid finite difference approach of Casulli and Walters (2000) with the finite element approach (Walters and Casulli, 1998). For the horizontal approximation, both use piecewise constant water elevation on a cell/element and normal velocity along the edges for the dependent variables. For the finite difference approach, gradients are calculated between circumcenters of the cells which maintains second-order accuracy but places constraints on the grid distortion. For the finite element approach, the gradients are effectively calculated along a normal between the centroid and element edge. For a regular grid, the approximations are identical; for a distorted grid, the finite difference approach theoretically maintains higher accuracy while the finite element approach does not have constraints on the distortion. There are additional differences in the approximation in the vertical direction.

The choice of vertical grid and approximation is very problem specific. The usual choice is between a level coordinate (z coordinate) and a terrain following coordinate (σ coordinate). For flow over steep terrain such as wave runup or river flow, level coordinates are somewhat hopeless to use and thus σ coordinates are used. Such is also the case when bottom boundary layers are of interest. However, z coordinates are much more accurate when calculating horizontal gradients, particularly density forcing, for the reasons given in Haney (1991). For my own purposes, I have adopted both approximations which perhaps makes the coding a bit messy. Probably a better approach is to use a generalised vertical coordinate such as described in some detail in Pietrzak et al. (2002). When using level coordinates it is also advisable to use some form of cut elements in order to avoid spurious effects from stepped depth (see for instance Rosatti et al., 2005).

Whichever vertical coordinate is used, linear bases are used to interpolate the velocity in the vertical (Walters, 1992). This is the lowest-order polynomial that can approximate the stress terms.

The choice of suitable advection schemes for unstructured grids is arguably the most significant problem with coastal ocean models. Most explicit, implicit, and semi-Lagrangian schemes have been tried somewhere at least once. One major problem is the wide range in Courant number ($Cr = u\Delta t/L$) encountered, and another is the difficulty in constructing higher-order approximations on unstructured grids. Some guidance in this endeavor is provided by Leonard (2002) who examines the stability of explicit and semi-Lagrangian advection formulations. In the end there are but two choices: traditional upwind schemes that are limited by Courant number and semi-Lagrangian schemes that are unconditionally stable. These schemes have also been analysed in several papers by Casulli (1987, 1990) where tracking methods, stability, artificial viscosity, and interpolation methods are considered.

Although semi-Lagrangian methods seem ideal, the proper choice of tracking and interpolation methods is crucial for maintaining accuracy. Some examples are shown in the following section. Low-order (linear) interpolation can lead to poor accuracy and oscillating behavior in the wetting and drying algorithm. Although high-order methods are well established for structured grids with regular quadrilaterals, they are difficult to implement on an unstructured grid (Staniforth and Côte, 1991; Le Roux et al., 1997). In a recent paper dealing with unstructured grids, Hanert et al. (2005) compared an explicit upwind scheme with a semi-Lagrangian scheme that uses a kriging interpolator. As an indication of efficiency, the semi-Lagrangian calculations were about ten times more expensive than the Eulerian calculations and both gave acceptable results for the large-scale test problems (Hanert et al., 2005).

A typical coastal ocean application with somewhat complicated geometry generally results in a wide range in velocity and hence in Cr. A large part of the grid can have small Cr and be amenable to explicit upwind methods along the lines suggested by Hanert et al. (2005). However, there may be other areas with jets or high velocity flows that are not stable under these schemes. As a result, we have chosen to implement both schemes with a switch from explicit upwind advection to semi-Lagrangian advection at a specified Cr. What appears to be missing at this time is a high-order upwind method that bridges the gap between these schemes.

5. Examples

The example presented here is meant to illustrate many of the tradeoffs that must be made in applying a coastal ocean model. The study area is the Kaikoura coastal margin (northeast coast, the South Island, New Zealand). For a study of coastal circulation with time scales of the order of the astronomical tides or longer, a relatively coarse resolution with long time steps would be used. This limit tends to favor many of the methods chosen for the numerical model such as improving the accuracy of the semi-Lagrangian advection approximation (Casulli, 1990) and allowing a relatively large CFL number.

In the other limit of short time scales are tsunami generated locally on the continental shelf. These waves are characterised by short wavelength ($\sim$10 km) and require higher resolution. Moreover, the accuracy of the wave height is of importance so that the CFL number must be kept small in the areas of interest. The resultant small time step size then leads to a less accurate set of conditions for the advection algorithm. During runup and rundown on the shore, the flow can become critical ($Fr = u/c > 1$) where Fr is the Froude number and c is phase speed. Finally, the waves are weakly dispersive so non-hydrostatic forces must be accounted for. After a brief description of this application, these points will be discussed.

The original objective of this case study was an assessment of the potential impact of tsunami events on the Kaikoura District coastal margins (northeast coast, the South Island, New Zealand), and what hazards they pose to lifelines (Walters et al., 2006). The study area extends from Oaro in the south, to Kekerengu in the north, including the populated area around Kaikoura Peninsula (Fig. 1). Subsequently, this case study has become a challenging problem for evaluating numerical methods.

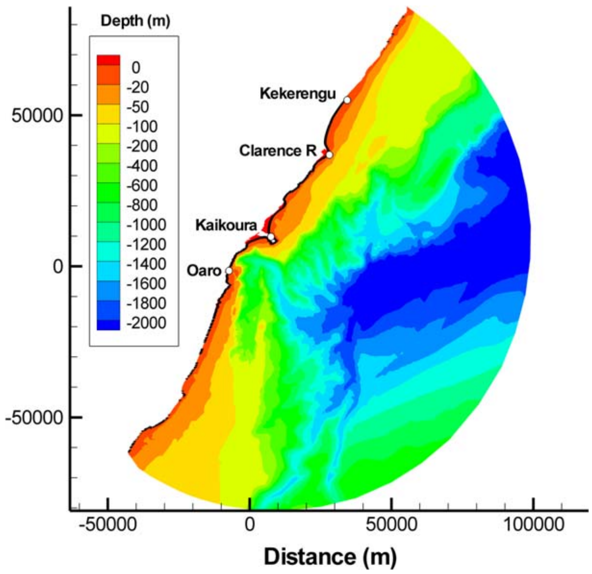

Fig. 1. Water depth along the Kaikoura coast. The head of the submarine canyon is at 173.6E longitude and 42.5S latitude. For scale, the coastline is 200 km long. The black line denotes the shoreline (mean sea level).

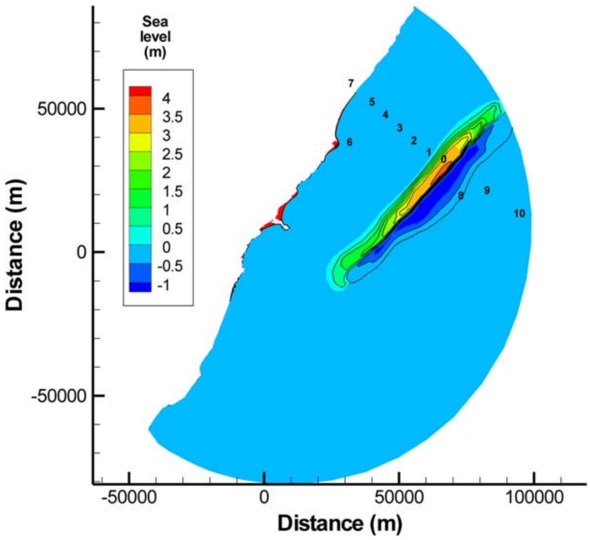

Fig. 2. Specified initial water surface elevation from a rupture on the Kekerengu Bank Fault. Sites where sea level is plotted in Fig. 5 correspond to the numbered symbols along the path of wave propagation. A black line denotes the shoreline (mean sea level).

A major threat to this area is from a tsunami generated by a potential rupture of the Kekerengu Bank Fault (Fig. 2). The northwest-dipping Kekerengu Bank thrust is located at a water depth of about 1000–1500 m on the continental slope. This fault has a late quaternary slip rate that can be estimated, on the basis of its bathymetric expression, to be of the order 0.5–1.5 mm/year.

Normally, fault movement is rapid when compared to time scales for wave propagation. Thus, due to the incompressible nature of water, the instantaneous initial conditions on the water surface are the same as the fault displacement. Essentially, the tsunami starts with zero velocity and a surface displacement given by the estimates for seabed rupture, and the wave evolves in time as a long gravity wave. At the open (sea) boundaries, a radiation condition is enforced so that the outgoing wave will not reflect back into the modelled area.

The initial bottom displacement is about 3 m in the landward overthrust area and -1 m in the seaward underthrust (Fig. 2). The resultant wave decomposes into two waves moving in opposite directions, one moving onshore that causes runup and one moving offshore that is radiated outward at the open boundaries (Fig. 3). The landward propagating tsunami primarily affects the area from Clarence River northward, with maximum runup heights of about 7 m. Fig. 3 shows a time sequence of water surface elevation during the simulation where snapshots of sea level at 100 s intervals are superimposed. In particular, the initial wave is near the center of the figure and propagates both onshore and offshore. Shoaling effects on the onshore propagating wave are can be seen by the increased wave height and decreased wavelength.

Most of the area is affected by the primary wave with a period of about 3 min, and there are minor waves for several hours afterward. However, when the primary wave reflects from the coast, it forms an edge wave which then travels down the coast and eventually excites a resonance near Kaikoura. The largest waves at Kaikoura (about 1.5 m) have a 10-min period and appear about 1.5 h after the tsunami was generated (Walters et al., 2006).

The initial wave was discretised with approximately 20 elements across the wave in a direction normal to the shoreline. The characteristic edge length is 400 m at the initial wave, reducing to 20 m along the shoreline, and increasing to 1 km at the outer boundary. The resultant grid has slightly over 1 million elements. It is not possible to generate a useful grid with a constant CFL number because of constraints on element gradation and highly variable bottom topography. Hence, the design criterion was to maintain low CFL number shoreward of the initial wave and have larger CFL number (and less accuracy) for the radiated wave. The final time step size was 1 s, certainly much smaller than would be chosen for a larger scale and longer period application. However, this size was required to give an accurate representation of the incident wave at the shoreline.

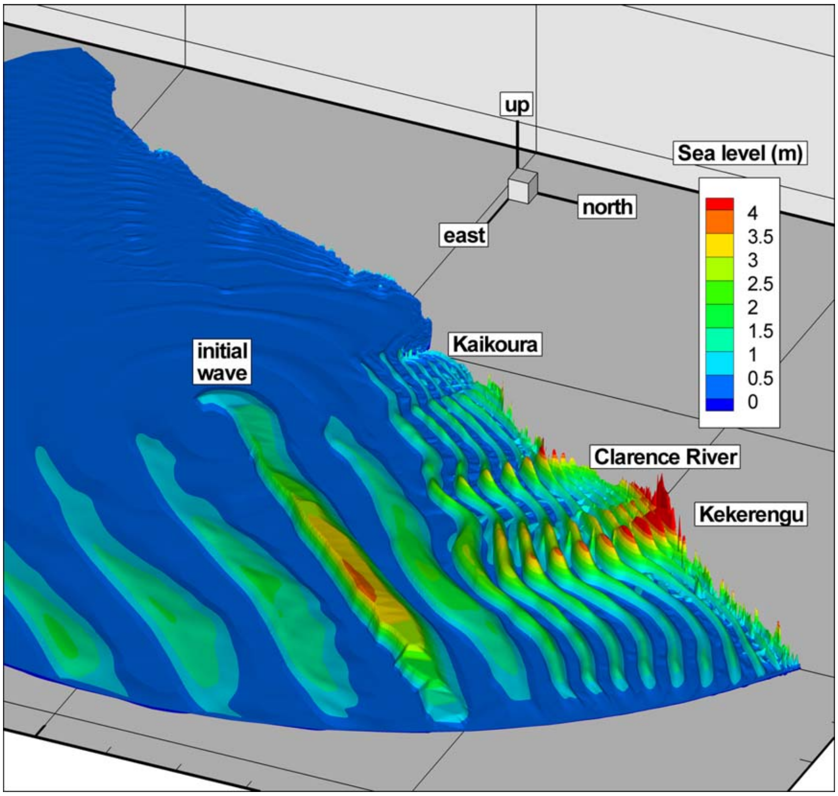

Fig. 3. Time sequence of water levels at 100 s intervals for a tsunami generated by a Kekerengu Bank fault-rupture. (*Note*: the entire semi-circular model domain is shown with Kaikoura Peninsula at the circle's centre.)

Because of the wide range in Cr, often exceeding 1, there were numerous difficulties with the advection approximations that led to experimenting with a low Cr upwind scheme and a high Cr semi-Lagrangian scheme. A typical set of results at points 6 and 7 in Fig. 2 is shown in Fig. 4. Scheme 1 is the case with

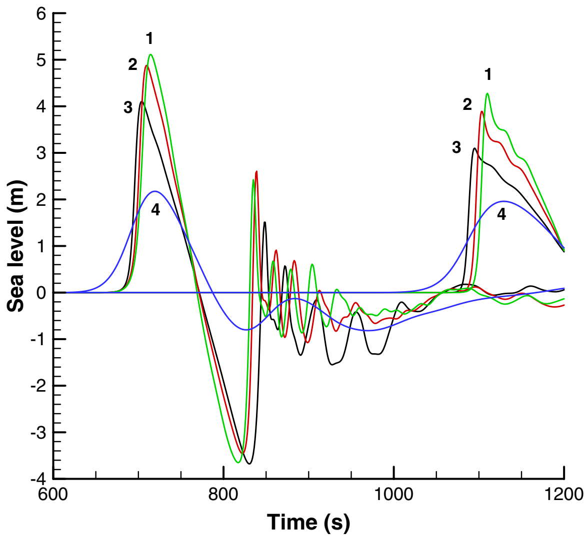

Fig. 4. Results for several interpolation schemes for the semi-Lagrangian advection method: (1) no advection; (2) linear interpolation from local bases; (3) interpolation from adjacent elements; (4) interpolation from global velocity.

advection neglected. Scheme 2 is semi-Lagrangian advection with linear interpolation locally within the element that contains the departure point. Scheme 3 is the same except that the interpolation is based on linear interpolation of the edge values of the adjacent triangles. Scheme 4 is the same except that the linear interpolation is based on the globally reconstructed velocity at the nodes. The results for the upwind scheme are similar to Scheme 2. With these low-order interpolation methods, there is a dramatic damping of the wave that increases with the size of the stencil. Moreover, Scheme 2 led to unphysical oscillations in wetting and drying and that particular combination of methods was not robust. Obviously, there needs to be additional work to sort out the details.

Using the width of the fault displacement as an estimate of wavelength, the depth to wavelength ratio is about 0.1 ($kH = 0.6$) or slightly above the upper limit of shallow water theory. However, the wave contains shorter wavelength components due to an asymmetric distortion on the fault so this estimate is probably too low.

The primary interest here is in the surface wave so that a depth-averaged single layer approximation is used. Non-hydrostatic effects are included through a vertical average of the Navier–Stokes equations following the methods described by Stelling and Zijlema (2003). This basic procedure has been incorporated into a semi-implicit finite element model (RiCOM, River and Coastal Ocean Model) and tested for a variety of dispersive wave problems (Walters, 2005b).

The sites identified by symbols in Fig. 2 are numerical water level gauges where the results from the various model approximations are compared. For the shoreward propagating wave, the model results are compared for the shallow water model and the non-hydrostatic model in Fig. 5.

Initially, the water elevation is specified (Fig. 2) and the velocity is zero. This initial condition gives rise to two waves propagating in opposite directions. The shoreward propagating wave shoals and the wave slows and increases in height. The differences in the results from the shallow water version and the non-hydrostatic version of the model are due to the dispersive nature of the waves (Fig. 5). Initially the trailing side of the wave is steeper because of the initial wave shape. For the shallow water version, phase speed is only dependent on the height of the wave so the crest travels faster than the trailing slope and the entire wave steepens on its forward face as it propagates shoreward (from 0 to 6 in Fig. 5). For the non-hydrostatic version, the short wavelength components have a slower phase speed and the wave attains a form similar to a solitary wave. At the shoreward site (6 in Fig. 5), the wave height is about 20% smaller than the shallow water wave. When the waves have finally steepened into a bore, there is little difference in their height or shape (7 in Fig. 5).

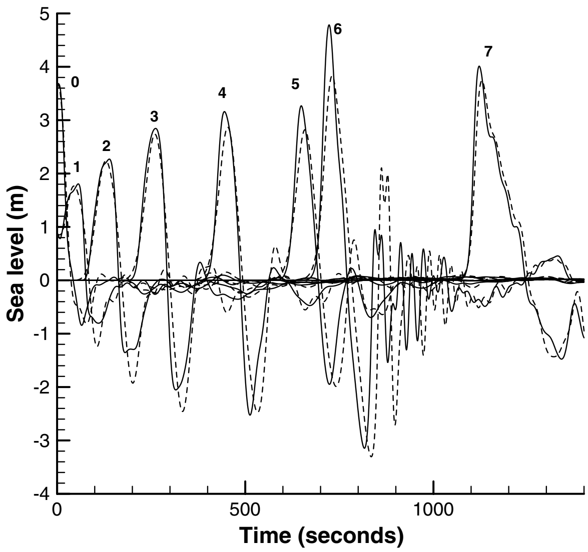

Fig. 5. Evolution of shoreward propagating tsunami. Shallow water version (solid), non-hydrostatic version (symbols).

As a result, dispersive effects significantly modify the shape of the tsunami for both the onshore and offshore propagating waves. Depending on location along the shore, the runup may be reduced slightly. However, the tsunami propagating offshore (a remote tsunami at a distant location), is modified considerably by dispersive effects.

6. Concluding remarks

Some design considerations for developing a coastal ocean model have been presented here. Several fundamental choices must be made: choosing the form of the governing equations, choosing a space and time discretisation, and selecting the particular physical processes to include. Of these, choice of discretisation (element and associated basis functions) and advection scheme are two longstanding issues in model development.

The choices presented here result in a model that is applicable to a wide range of time and space scales that are encountered in coastal oceanography. As time goes on and new applications emerge, these choices can be refined as necessary.

Acknowledgements

The research was partly funded by the New Zealand Foundation for Research Science and Technology (C01X0307 and CO1X0024). The Kaikoura tsunami study was partly funded by Environment Canterbury.

References

Bradford, S.F., Sanders, B.F., 2002. Modeling flows with moving boundaries due to flooding, recession, and wave run-up. In: Spaulding, M.L. (Ed.), Estuarine and Coastal Modeling: Proceedings of the 7th International Conference. ASCE, Reston, Virginia, pp. 695–708.

Burchard, H., 2002. Applied turbulence modelling in marine waters. Lecture Notes in Earth Sciences, vol. 100. Springer, Berlin, 215 pp.

Casulli, V., 1987. Eulerian–Lagrangian methods for hyperbolic and convection dominated parabolic problems. In: Taylor, C., Owen, D.R., Hinton, E. (Eds.), Computational Methods for Non-linear Problems. Pineridge Press, Swansea, pp. 239–268.

Casulli, V., 1990. Semi-implicit finite difference methods for the two-dimensional shallow water equations. J. Comput. Phys. 86, 56–74.

Casulli, V., 1999. A semi-implicit finite difference method for non-hydrostatic free surface flows. Int. J. Numer. Methods Fluids 30, 425–440.

Casulli, V., Cattani, E., 1994. Stability, accuracy, and efficiency of a semi-implicit method for three-dimensional shallow water flow. Comput. Math. Appl. 27 (4), 99–112.

Casulli, V., Walters, R.A., 2000. An unstructured grid, three-dimensional model based on the shallow water equations. Int. J. Numer. Methods Fluids 32, 331–348.

Casulli, V., Zanolli, P., 2002. Semi-implicit numerical modeling of nonhydrostatic free-surface flows for environmental problems. Math. Comput. Model. 36, 1131–1149.

Casulli, V., Zanolli, P., 2005. High resolution methods for multidimensional advection–diffusion problems in free-surface hydrodynamics. Ocean Model. 10, 137–151.

Finnigan, J.J., 2000. Turbulence in plant canopies. Annu. Rev. Fluid Mech. 32, 519–571.

Galperin, B., Orszag, S.A. (Eds.), 1993. Large Eddy Simulation of Complex Engineering and Geophysical Flows. Cambridge University Press, Cambridge, p. 600.

Hanert, E., Legat, V., Deleersnijder, E., 2002. A comparison of three finite elements to solve the linear shallow water equations. Ocean Model. 5, 17–35.

Hanert, E., Le Roux, D.Y., Legat, V., Deleersnijder, E., 2005. An efficient Eulerian finite element method for the shallow water equations. Ocean Model. 10, 115–136.

Haney, R.L., 1991. On the pressure gradient force over steep topography in sigma co-ordinate ocean models. J. Phys. Oceanogr. 21, 610–619.

Hua, B.L., Thomasset, F., 1984. A noise-free finite element scheme for the two-layer shallow water equations. Tellus A 36, 157–165.

King, I.P., Norton, W.R., Iceman, K.R., 1974. A finite element model for two-dimensional flow. In: Oden, J.T. et al. (Eds.), Finite Elements in Flow Problems. University of Alabama at Huntsville (UAH) Press, Huntsville, Alabama, pp. 133–137.

Le Provost, C., Rougier, G., Poncet, A., 1978. Numerical modeling of the harmonic constituents of the tides, with application to the English Channel. J. Phys. Oceanogr. 11, 1123–1138.

Le Roux, D.Y., Lin, C.A., Staniforth, A., 1997. An accurate interpolating scheme for semi-Lagrangian advection on an unstructured mesh for ocean modelling. Tellus 49 (A2), 119–138.

Le Roux, D.Y., Staniforth, A., Lin, C.A., 1998. Finite elements for shallow water equation ocean models. Mon. Weather Rev. 126, 1931–1951.

Leonard, B.P., 2002. Stability of explicit advection schemes. The Balance point location rule. Int. J. Numer. Methods Fluids 38, 471–514.
Lin, P., Li, C.W., 2002. A σ coordinate three-dimensional numerical model for surface wave propagation. Int. J. Numer. Methods Fluids 38, 1045–1068.
Lynch, D.R., Gray, W.G., 1979. A wave-equation model for finite-element tidal computations. Comput. Fluids 7, 207–228.
Lynch, D.R., Werner, F.E., 1991. Three dimensional hydrodynamics on finite elements. Part 2: Nonlinear time-stepping model. Int. J. Numer. Methods Fluids 12, 507–533.
Monin, A.S., Ozmidov, R.V., 1985. Turbulence in the Ocean. Reidel Pub. Co., Dordrecht, Holland, 247 pp.
Nikora, V., Goring, D., McEwan, I., Griffiths, G., 2001. Spatially-averaged open-channel flow over a rough bed. J. Hydraul. Eng. 127 (2), 123–133.
Phillips, O.M., 1969. The dynamics of the upper ocean. Cambridge Monographs on Mechanics and Applied Mathematics. Cambridge University Press, London, 261 pp.
Pietrzak, J., Jakobson, J., Burchard, H., Vested, H.J., Peterson, O., 2002. A three-dimensional hydrostatic model for coastal and ocean modelling using a generalised topography following co-ordinate system. Ocean Model. 4, 173–205.
Raviart, P.A., Thomas, J.M., 1977. A mixed finite element method for 2nd order elliptic problems. Mathematical Aspects of the Finite Element Method. Lecture Notes in Math. Springer, Berlin.
Rosatti, G., Cesari, D., Bonaventura, L., 2005. Semi-implicit, semi-Lagrangian modelling for environmental problems on staggered Cartesian grids with cut cells. J. Comput. Phys. 204 (1), 353–377.
Sani, R.L., Gresho, P.M., Lee, R.L., Griffiths, D.F., 1981. The cause and cure (!) of the spurious pressures generated by certain FEM solutions of the incompressible Navier–Stokes equations: Part 1. Int. J. Numer. Methods Fluids 1, 17–43.
Staniforth, A., Côte, J., 1991. Semi-Lagrangian integration schemes for atmospheric models—A review. Mon. Weather Rev. 119, 2206–2223.
Stelling, G., Zijlema, M., 2003. An accurate and efficient finite-difference algorithm for non-hydrostatic free-surface flow with application to wave propagation. Int. J. Numer. Methods Fluids 43, 1–23.
Walters, R.A., 1992. A 3D, finite element model for coastal and estuarine circulation. Cont. Shelf Res. 12 (1), 83–102.
Walters, R.A., 2005a. Coastal ocean models: two useful finite element methods. Cont. Shelf Res. 25, 775–793.
Walters, R.A., 2005b. A semi-implicit finite element model for non-hydrostatic (dispersive) surface waves. Int. J. Numer. Methods Fluids 7, 721–737.
Walters, R.A., Barnes, P., Lewis, K., Goff, J., 2006. Locally generated tsunami along the Kaikoura coastal margin: Part 1. Fault ruptures. New Zeal. J. Marine Freshwater Res. 40 (1), 1–16.
Walters, R.A., Carey, G.F., 1984. Numerical noise in ocean and estuary models. Adv. Water Resour. 7, 5–20.
Walters, R.A., Casulli, V., 1998. A robust, finite element model for hydrostatic surface water flows. Commun. Numer. Methods Eng. 14, 931–940.